Journal of Nanophotonics

Nanophotonics.SPIEDigitalLibrary.org

Efficient and stable thin-film crystalline silicon solar cell by introducing rotation factor in surface square pillar array grating

Jin Hou
Binxian Yang
Xiaohang Li
Can Ma
Bing Wang
Hao Long
Chunyong Yang
Shaoping Chen

SPIE.

Jin Hou, Binxian Yang, Xiaohang Li, Can Ma, Bing Wang, Hao Long, Chunyong Yang, Shaoping Chen, "Efficient and stable thin-film crystalline silicon solar cell by introducing rotation factor in surface square pillar array grating," *J. Nanophoton.* **14**(1), 016008 (2020), doi: 10.1117/1.JNP.14.016008

Efficient and stable thin-film crystalline silicon solar cell by introducing rotation factor in surface square pillar array grating

Jin Hou,[a,*] Binxian Yang,[a] Xiaohang Li,[b] Can Ma,[a] Bing Wang,[c] Hao Long,[a] Chunyong Yang,[a] and Shaoping Chen[a]

[a]South-Central University for Nationalities, College of Electronic and Information Engineering, Hubei Key Laboratory of Intelligent Wireless Communications, Wuhan, China

[b]King Abdullah University of Science and Technology, Advanced Semiconductor Laboratory, Thuwal, Saudi Arabia

[c]Sun Yat-Sen University, School of Electronics and Information Technology, Guangzhou, China

Abstract. To obtain efficient and stable light trapping, angle rotation is introduced to form rotated square pillar array grating (SPAG) solar cells. Compared with the unpatterned stack slab and the optimized uniform SPAG cells, the maximum short-circuit current (J_{sc}) of the optimized rotated SPAG is increased by 78.54% and 3.21%, respectively. Moreover, besides the fact that the low-incidence angular sensitivity of J_{sc} could be maintained, J_{sc} of the optimized rotated SPAG will always be larger than that of the optimized uniform SPAG at any incident angle. Furthermore, when the structural parameters of the subsquare pillar slightly deviate from the optimum, the absorption only deceases slightly as well, which indicates both a high structural tolerance and a stable absorption performance. In addition, our results show not only that the proposed rotated SPAG is promising to make light trapping efficient and stable but also that introducing rotation disorders is promising for other high-absorption pseudounordered surface structures. © *2020 Society of Photo-Optical Instrumentation Engineers (SPIE)* [DOI: 10.1117/1.JNP.14.016008]

Keywords: photovoltaic; subwavelength structures; nanostructures; diffraction gratings; solar energy.

Paper 19110 received Aug. 24, 2019; accepted for publication Jan. 21, 2020; published online Feb. 8, 2020.

1 Introduction

Thin-film crystalline silicon (c-Si) solar cells are considered as one of the most promising cost-effective photovoltaic cells due to less material consumption.[1–3] However, the active layer, which is much thinner than the c-Si absorption length, can lead to poor optical absorption. Therefore, various ordered nanostructures, such as gratings,[4–9] array gratings or photonic crystals,[2,10–12] plasmonic metal structures,[13,14] and biomimetic structures,[15–17] have been proposed on the front, rear, or both sides of the absorbing material layer to enhance the optical absorption. Specifically, although a few guided mode resonances excited in ordered structures result in increase of light absorption, compared with the wide absorption spectrum of c-Si, their high absorption spectrum bandwidths are still very limited. Later, some disordered surface structures with a richer Fourier spectrum, which could increase the number of accessible diffraction orders for scattering, are found to be able to further enhance the absorption bandwidth.[3,18] However, how to design deliberated true disordered structures is complicated and time-consuming. Their fabrications are also very challenging, thus limiting the practical utilizations.[19] Conversely, design and fabrication of conventional ordered structures, which comprise simple single and regular composition structural elements, are relatively easier. Thus, multiple structures that have features of both locally disordered and long-range ordered have been proposed to combine the advantages of both periodic and random domains, such as quasirandom nanostructures,[20–24] pseudodisordered

*Address all correspondence to Jin Hou, E-mail: houjin@mail.scuec.edu.cn

1934-2608/2020/$28.00 © 2020 SPIE

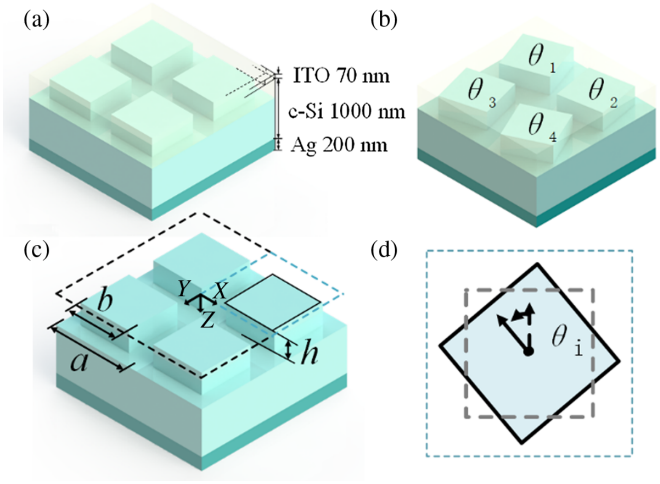

Fig. 1 Schematic view of the thin-film c-Si solar cells. (a) Uniform SPAG cell, (b) 2×2 supercell rotated SPAG cell, (c) uniform SPAG cell without the ITO layer depicted and with characteristic parameters of SPAG denoted, and (d) top view of a rotated pillar and the gray dotted line is the outline of an unrotated pillar.

structures,[1,25–28] and quasicrystal structures.[29,30] As a straightforward implementation method, most pseudodisordered structures are designed by introducing local structural disorders in finite periodic array structures, such as arrays of round holes,[3,25,27] cylinders,[31] cuboids,[32] inverted pyramids,[19,26] and moth eyes.[1] It is found that the method is useful to further increase the light-capture ability. Although the pseudodisordered structure has appeared in various styles,[1,3,25–27,31,32] generally speaking, the ways used to form local disorders can be dissected in the two main categories. One is by setting different shape parameters for each substructure,[1,26,31,32] and the other is by changing the relative positions between the substructures.[1,25–27] In addition to the two categories, previous investigations of ordered structures indicate that the angle rotation is also an important factor for enhancement of optical absorption and interaction.[10,33–37] Compared with the mentioned two categories, the way of introducing rotation as disorders in array structures has two features. First, the invariable substructural center position in rotation is similar to the case of changing shape parameters. Second, the invariable substructural shape in rotation also has similarity to the case of changing relative position. Thus, the rotation as a disorder factor should be regarded as another kind of structure category and it may have distinguished significance in adjusting light trapping, which would inherit merits from changing both shape and position parameters. However, to date, the rotation as a structural variation factor to form pseudodisordered structures has not been systematically studied to enhance light absorption.

To verify whether rotation is efficient for optical absorption enhancement, in this paper, rotation is considered as an unordered factor to generate local disorders in the square pillar array grating (SPAG). First, an optimized uniform SPAG without rotation is designed, with structural parameters that could obtain maximum short-circuit current (J_{sc}). To be used as the basis for rotation, the optimized uniform SPAG is chosen with a structural size restriction where the square pillars in SPAG could be freely rotated without overlapping with neighbors. Then, various angle rotations of the subsquare pillars in the 2×2 supercell of the SPAG are randomly introduced, creating local disorders to form the rotated SPAG according to an equal probability categorical distribution. To obtain the best range of rotation angle for larger J_{sc} by larger probability, J_{sc} values as a function of both the mean and the standard deviation of the rotation angles of subsquare pillars in the rotated SPAG are thereafter investigated. Moreover, compared with the optimized uniform SPAG, maximum J_{sc} of 27.394 mA/cm^2 for the optimized 2×2 rotated SPAG cell is obtained, which shows that suitable rotation would further enhance light-capture ability. Afterward, absorption spectrum comparison, diffraction order analysis, and field distribution investigation are successively presented to understand why the rotated SPAG could obtain high-absorption efficiency. Furthermore, incident angle characteristics and structural tolerance of

the rotated SPAG solar cell are discussed. In addition, taking rotation as the local disorders structural factor, a new rotated spiral grating cell is designed to illustrate how angle rotation could further enhance light absorption based on the other geometric structures.

2 Design and Investigation Methodology

To conveniently introduce local rotation disorders, the usual square pillar shape shown in Fig. 1(a) is chosen as the basic structure. Compared with inverted pyramid,[9,26,35] elliptic cylinders,[33,36] and other complex composite structures[10,38] in which local rotation disorders could also be introduced, the square pillar not only can be fabricated easily but also has a 90-deg rotational symmetry. The rotational symmetry of the square pillar could reduce the calculation complexity during the design stage. Thus, it is deemed as the worth investigation. As shown in Fig. 1(a), four subsquare pillars arranged in a square array are used to form a supercell of the 2×2 SPAG. In the supercell, local rotation disorders are then introduced by rotating each subsquare pillar with a random angle in the horizontal plane, as shown in Fig. 1(b). The SPAGs are located on the surface of the c-Si layer. Below the c-Si layer, silver (Ag) is used as a reflection layer. On the upper side of the rotated SPAG, indium tin oxide (ITO) is coated as the antireflection layer. The conducting ITO layer and the Ag layer also can drive the current generated in the absorbing material c-Si.

In this paper, we concentrate on the rotation properties of the SPAGs; therefore, a uniform SPAG without rotation as the reference should be first determined. Most essential structural parameters of the uniform SPAG are chosen referenced to previous investigation results.[3,39–42] The thicknesses of the ITO layer, c-Si (including the SPAG) layer, and Ag layer are set to 70,[18,39] 1000,[3,39] and 200 nm,[3,22,39] respectively. Their optical properties are taken from the literatures.[40–42] Especially, the extinction coefficient of ITO is set to 0 to simplify the absorption calculation of the c-Si material. The Ag layer in the proposed solar cell is used as a back contact and also as a backside reflector. In the calculation model, both light absorption in the Ag layer and reflection at the Ag layer surface have been taken into considerations. The thickness of 200 nm is set to ensure that no light transmits through the Ag layer.[3,22,39] The distance between the centers of two neighboring square pillars a is fixed at 600 nm, because good absorptions have been demonstrated with this value.[43,44] Hence, the square pillar height h and its width b are still unfixed as key structural parameters of the uniform SPAG. In Sec. 3.1, J_{sc} dependence studies of these two parameters are performed to determine the optimized uniform SPAG. As shown in Fig. 1(c), the coordinate system of the solar cell is depicted. The origin point is located at the center of the top ITO layer. The directions of X and Y are along the direction of the period, respectively. The direction of Z is from top to bottom.

After the optimized uniform SPAG is determined, local rotation disorders are introduced by rotating subsquare pillars around their own center vertical line with some specific angles. The top view of a rotated subsquare pillar is shown in Fig. 1(d), in which the square center point is used as the rotation center and counterclockwise is the positive rotation direction. For the choice of the supercell size, generally speaking, there would be better absorption performance in a larger supercell with more degrees of freedom. However, the increase of absorption would not be linearly proportional to the increase of degrees of freedom. In fact, the increase of absorption is more dependent on the disorders that are introduced. When the disorders are increased to some degrees, the absorption will get to be saturated. For the case where the 2×2 supercell is increased to the 3×3 supercell, only a few disorders would be added in the same area. Therefore, the absorption would not increase greatly. Similar comments could be found in the study of Ding et al.,[25] in which introducing position disorders are investigated. Moreover, the calculation of larger supercells will take a long time for our computing resources. Therefore, in this paper, a 2×2 supercell is chosen to investigate rotation properties instead of larger supercells. In the 2×2 supercell, the rotation angles of the four subsquare pillars are defined as θ_1 to θ_4, respectively, as shown in Fig. 1(b). To decrease calculation time, due to the 90 deg rotational symmetry, the rotation angle range considered could be simplified to -45 deg to 45 deg. Within this range, angle elements are selected with equal interval, which constitute an alternative angle set to generate random rotation of subsquare pillar subsequently. The four angles of the four sub square

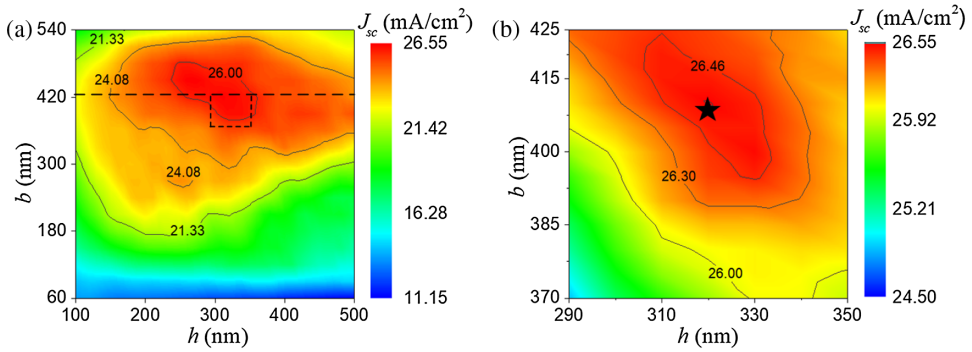

Fig. 2 J_{sc} of the uniform SPAG solar cell as a function of h and b. (a) The result for larger parameter range and (b) the high resolution result for smaller parameter range, which is enclosed by a rectangular dashed line in (a). The horizontal dashed line indicates the maximum b value, below which the square pillars can arbitrarily rotate without overlapping. Solid pentagram is the optimized point.

pillars of a supercell will be successively determined from discrete rotation angle range by an equal probability categorical distribution, $\theta \sim \mathrm{Cat}(1/n)$, where n is the number of discrete angle elements in the rotation range. In this paper, all n is set at 7 to decrease complexity. Then, the subsquare pillars in the supercell of SPAG cell will be rotated accordingly to induce local disorders.

For the numerical calculation, rigorous coupled-wave analysis[45] is adopted to obtain the reflectance and transmittance of the c-Si absorption material in the wavelength range of 300 to 1000 nm. If not specified, J_{sc} obtained is under normal incidence with unpolarized light (average of TE and TM), and it is given as

$$J_{sc} = \frac{e}{hc}\int_{300}^{1000} \lambda[1 - R(\lambda) - T(\lambda)]S(\lambda)\mathrm{d}\lambda, \tag{1}$$

where e, h, c, R, T, and S are the electron charge, the Planck constant, the speed of light in vacuum, the reflectivity, the transmittance, and the spectral density of the photon irradiance from the global AM 1.5 spectrum, respectively.[20,23,25,46,47]

3 Numerical Results and Discussion

3.1 *Uniform SPAG Optimization*

To select an appropriate uniform SPAG for subsequent studies, dependence studies on the key surface structural parameters (h and b) of subsquare pillar in the uniform SPAG solar cell are performed. J_{sc} values of the uniform SPAG solar cell as a function of h and b are plotted in Fig. 2. Here, h is varied with a fixed interval of 10 nm in a range from 100 to 500 nm, because within this range similar structures have demonstrated good absorptions.[48] Considering that a is fixed at 600 nm, b is first varied with an interval of 30 nm in a large range from 60 to 540 nm to find the approximate value to obtain large J_{sc}. To avoid the overlap of adjacent square pillars during rotation, b is limited to no more than $\sqrt{2}a/2$, which is about 424.26 nm and is marked with a horizontal dashed line in Fig. 2(a). Therefore, the preliminary optimized zone to obtain larger J_{sc} could be determined, and it is denoted by a rectangular dashed line in Fig. 2(a). Later, more accurate calculations are conducted at this zone, and this time the b is varied with a smaller interval of 5 nm in a range from 370 to 425 nm. The calculation result is shown in Fig. 2(b), and the largest J_{sc} of 26.54 mA/cm^2 identified by a solid pentagram is obtained in an optimized uniform SPAG cell with $b = 410$ nm and $h = 320$ nm, which will be subsequently used as the basis to design rotated SPAG.

Table 1 Results of random angle optimization for rotated SPAG.

Range and interval	Best J_{sc} (mA/cm^2)	Additional enhanced J_{sc} compared with optimized uniform SPAG (mA/cm^2)	Additional enhanced J_{sc} compared with optimized uniform SPAG (%)	Angle combination (θ_1, θ_2, θ_3, and θ_4) for best J_{sc}
−45 deg to 45 deg, 15 deg	27.267	0.726	2.74	(0 deg, 15 deg, 30 deg, and 15 deg)
−30 deg to 30 deg, 10 deg	27.349	0.808	3.00	(−10 deg, −20 deg, −20 deg, and −30 deg)
0 deg to ±30 deg, 5 deg	27.382	0.841	3.17	(10 deg, 25 deg, 25 deg, and 20 deg)

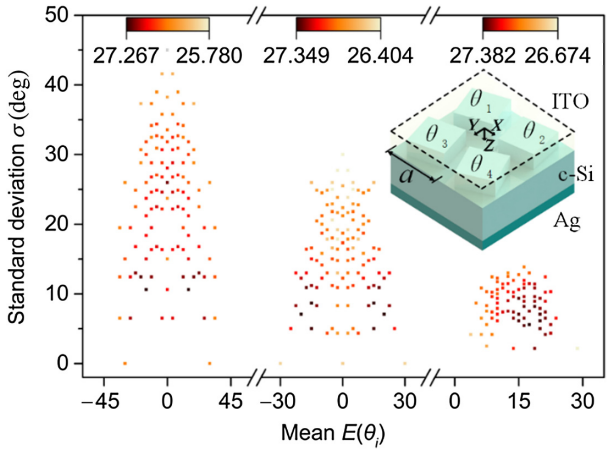

Fig. 3 J_{sc} of the rotated SPAG cell as a function of the mean and standard deviation for θ_1, θ_2, θ_3, and θ_4 at different rotation ranges. Because the structures with opposite rotation angles have the same J_{sc}, symmetric result points are complemented in the figure for a clearer demonstration. Illustration is the schematic view of the rotated SPAG solar cells.

3.2 *Rotated SPAG Optimization*

After the optimized uniform SPAG is obtained, a random method is adopted to introduce rotation angle disorders. First, as discussed in Sec. 2, four square pillars are used as a 2×2 supercell to introduce random rotation factors. To generate random rotation angles conveniently, every rotation angle in the supercell is in turn randomly selected from a candidate rotation set by an equal probability categorical distribution. Then, J_{sc} values of the 2×2 rotated SPAG cells represented by angle combinations are investigated to obtain high-performance 2×2 rotated SPAG cells. However, finding the four rotation angles of an optimized rotated SPAG cell in a wide rotation angle range requires lots of calculation resources and time. Therefore, ameliorating the rotation angle range based on some preliminary calculations would be more feasible.

For the rotated SPAG structures, because the pattern designs are obtained using a pseudorandom number-generator process, the statistic parameters of the rotated SPAG tend to be more important and need to be paid more attention. In such cases, the ameliorating design method considering statistic parameters is more preferable. Therefore, in the optimization process of stochastic computation, 100 different rotated SPAGs in each rotation range are randomly selected and calculated, which should be sufficient to find a plurality of high-efficient rotated SPAGs.[1,25] The maximum J_{sc} in each rotation range and its corresponding angle combination are provided in Table 1. To better demonstrate the effect of introducing rotation, the mean $E(\theta_i)$ and the standard deviation σ of the rotation angles θ_1 to θ_4 for each rotated SPAG are calculated. J_{sc} as a function of both $E(\theta_i)$, and σ is shown in Fig. 3.

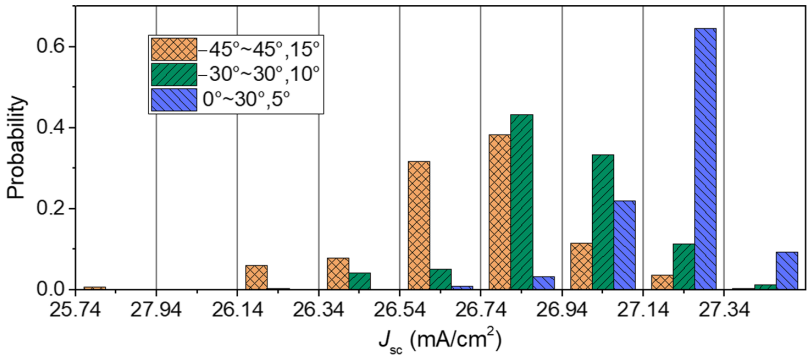

Fig. 4 Probability distributions of the angle combination numbers related to different J_{sc} levels for the three different rotation angle ranges. Different rotation ranges are distinguished by different colors and stripes.

With the decrease of the rotation range, the value of maximum J_{sc} increases accordingly, the maximum J_{sc} obtained by stochastic computation is 27.384 $\mathrm{mA/cm^2}$. Moreover, the amount of dark-red points with larger J_{sc} also increases with the decrease of the rotation range. Dark-red points tend to likely distribute in the mean range of 10 deg to 25 deg (range of -10 deg to -25 deg is the same for symmetry) with σ smaller than 15 deg. The phenomena indicate that the degree of angular rotation disorder should not be too large. In addition, to obtain a high absorption, all subsquare pillars should be only rotated with the same direction.

To ensure the ameliorating design method is efficient, J_{sc} values of all possible angle combinations in each rotation angle ranges are additionally calculated by the ergodic calculative method. As shown in Fig. 4, for the three different rotation angle ranges, probability distributions of the angle combination related to the specific J_{sc} level are plotted. The probability at each J_{sc} level is obtained by dividing the amount of angle combinations appearing at the specific J_{sc} level with the total possible angle combination amount. For rotation ranging from -45 deg to 45 deg, compared with optimized uniform SPAG, probabilities of only 3.9% and 0.3% are found when absorptions above 2.3% and 3% are obtained, respectively. When the rotation range is ameliorated to the range from -30 deg to 30 deg, probabilities of 12.7% and 1.3% are obtained to increase the absorption above 2.3% and 3%, respectively. When the rotation range is further ameliorated to the range from 0 deg to 30 deg, probabilities of 73.8% and 9.3% are obtained to increase the absorption above 2.3% and 3%, respectively. From the above probability distributions obtained by the ergodic calculative method, the probability of obtaining a large J_{sc} is significantly improved amid the amelioration of the rotation range, which is consistent with the phenomena shown in Fig. 3.

Therefore, the ameliorating design method to reduce the calculation is very efficient to find a highly absorptive rotated SPAG. Specially, the maximum J_{sc} obtained by this optimized ergodic calculative method is 27.394 $\mathrm{mA/cm^2}$, which is also very close to the maximum J_{sc} obtained by the upper ameliorating design method. We will use it in the subsequent analysis.

3.3 *Spectra Analysis of the Optimized Rotated SPAG Cell*

To understand why high-absorption performance of the rotated SPAG solar cell could be obtained, the absorption spectra of the optimized rotated SPAG, the optimized uniform SPAG, and the stack slab cells are compared in Fig. 5. Both the single-pass absorption[9] and the Yablonovitch limit[49] of 1000-nm c-Si slab are presented in the figure as well. For most of the wavelength range from 300 to 1000 nm, compared with the unpatterned stack slab cell, obvious improvements of absorption spectra have been found for both the optimized rotated SPAG and the optimized uniform SPAG cells. Compared with the absorption spectra of rotated SPAG cell with that of uniform SPAG cell, most part of the two absorption spectra are very close for the wavelength range from 300 to 750 nm. For the other longer wavelength range from 750 to 1000 nm, compared with the absorption spectra of the uniform SPAG cell, there are some higher and additional peaks at multiple wavelengths in the rotated SPAG cell absorption spectra. This is

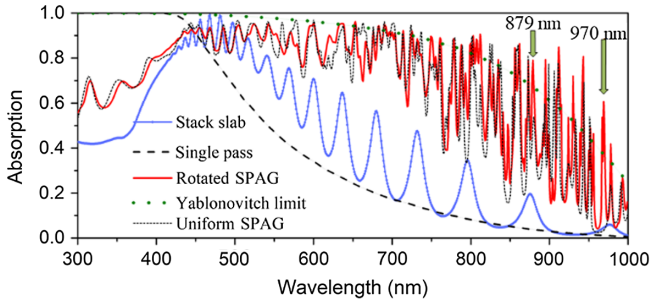

Fig. 5 Absorption spectra of the optimized rotated SPAG, the optimized uniform SPAG, and the stack slab cells, the Yablonovitch limit (green dotted line), and the single-pass absorption spectra (black dashed line) are provided.

due to the appearance of small local rotation disorders in the rotated SPAG cell, which may bring additional resonance in longer wavelength range.[27,50] Therefore, in the whole wavelength range, the overall absorption of the rotated SPAG cell is higher than that of the uniform SPAG cell. Compared with J_{sc} (15.343 mA/cm^2) obtained in the conventional unpatterned stack slab solar cell, J_{sc} (27.394 mA/cm^2) obtained in the rotated SPAG solar cell is increased by 78.54%. Moreover, compared with J_{sc} (26.541 mA/cm^2) obtained in the optimized uniform SPAG solar cell, an increase of 3.21% in the maximum J_{sc} could be obtained in the optimized rotated SPAG cell. This increase is comparable to surveys[25,27] with similar period and absorption layer thickness, in which 2% and 2.83% absorption enhancement were reported.

3.4 *Diffraction Orders and Field Analysis*

To further reveal the physical mechanism of higher and additional peaks in the absorption spectrum of the rotated SPAG solar cell in Fig. 5, the z axis positive component of the integral power (Poynting) flux density (PFD) of each diffraction order at the bottom plane of the rotated SPAG is compared with that of the uniform SPAG, as shown in Fig. 6. Two typical absorption peak wavelengths of 879 and 970 nm, marked with arrows in Fig. 5, are considered for investigation.

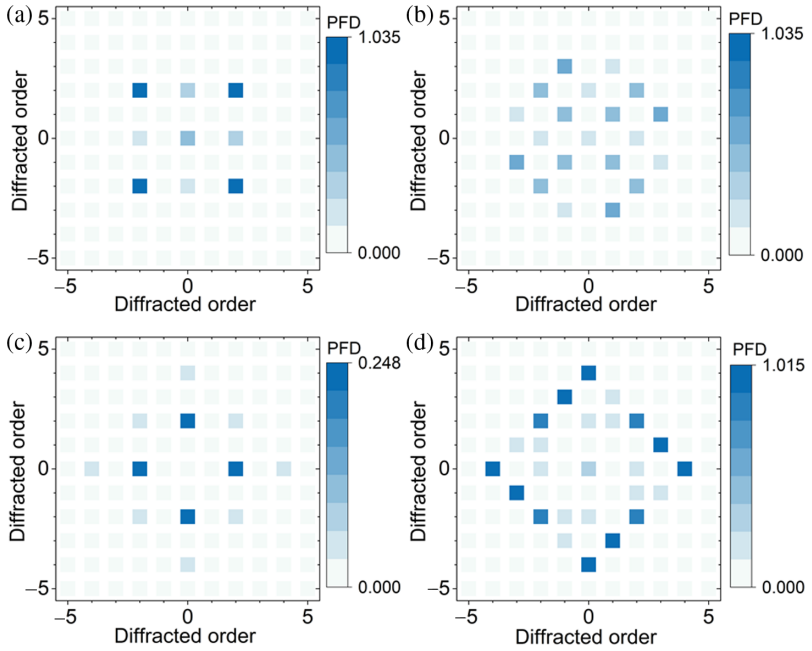

Fig. 6 The PFD for each diffraction order at the bottom plane of (a), (c) the uniform SPAG and (b), (d) the rotated SPAG. Subfigures (a) and (b) are calculated at 879 nm, (c) and (d) are calculated at 970 nm. The unit of PFD is arbitrary and the magnitudes of PFD are indicated by the color scales.

At 879 nm, shown in Fig. 6(a), only a few diffraction orders of the uniform SPAG are observed with large PFD values, whereas more diffraction orders of rotated SPAG are observed with unneglectable PFD values shown in Fig. 6(b). Therefore, compared with the uniform SPAG, the rotated SPAG not only diffracts light into more orders but also concentrates more diffraction energy into those orders with the addition of rotation disorders.[23] These additional diffractions can excite more quasiguided modes. The quasiguided modes can be more easily coupled into silicon. Thus, the reflection from the rotated SPAG will be reduced, which therefore leads to an increase in absorption.

Moreover, the propagating directions of higher-order diffractions are usually much more inclined than those of the lower orders, resulting in an increase of optical path in the absorptive silicon layer, which leads to absorption enhancement. Thus, in Fig. 5, at 879 nm, a higher peak in the absorption spectra of the rotated SPAG cell than that of the uniform SPAG cell is observed. For 970 nm, the phenomenon discussed above is more obvious as shown in Figs. 6(c) and 6(d). More high diffraction orders of rotated SPAG PFDs are observed with large PFD values. However, for uniform SPAG, there are low PFD values in all the diffraction orders, as shown in the color scale at the bottom of Fig. 6(c). Therefore, for 879 nm, the addition of rotation disorders in the rotated SPAG solar cell will lead to a high additional absorption peak at 970 nm as well. Thus, both higher and additional absorption peaks in Fig. 5 could be explained by the analysis of PFD for each diffraction order.

To intuitively show how the rotation disorders could boost the absorption enhancement at 970 nm, the electric field intensity distribution in the rotated SPAG cell is also compared with that in the uniform SPAG cell, as shown in Fig. 7. To clearly illustrate the effect of angle rotations in the SPAGs, the electric field intensity profiles in the $X-Z$ plane at both the projections and the grooves of the two different SPAGs are investigated. For uniform SPAG, the electric field intensity distributions are relatively simple, and low dark-red electric field intensities could be found in the Si layer, which indicates less modes and energies of light excited in the uniform SPAG solar cell, as shown in Figs. 7(a) and 7(b). This phenomenon is consistent with the results in Fig. 6(c), where a few low diffraction orders could be observed with low PFDs. As a comparison, in Figs. 7(c) and 7(d), the electric field intensity distribution of rotated SPAG solar cell is

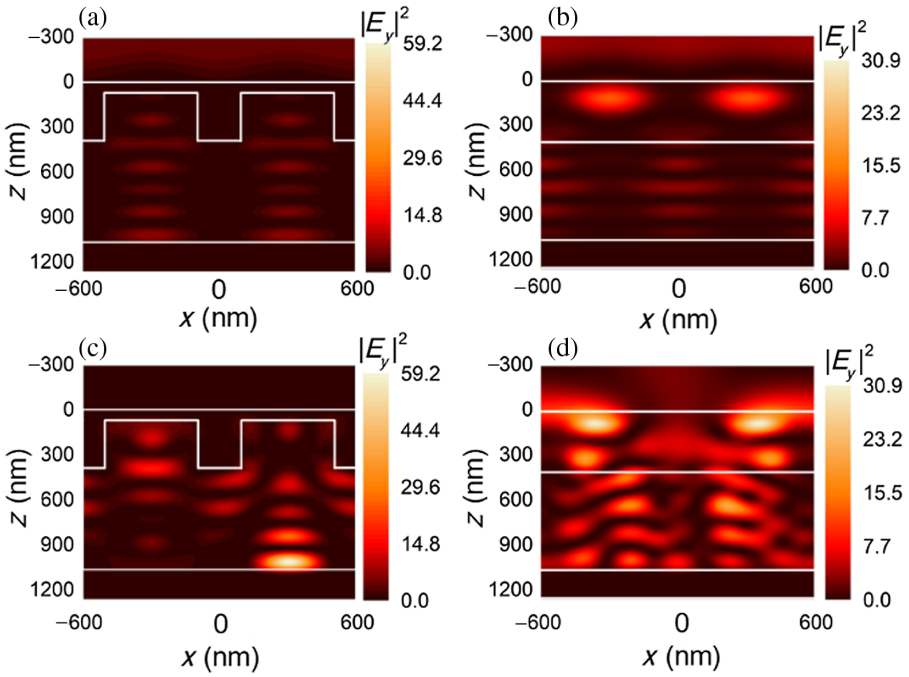

Fig. 7 Electric field intensity profiles at 970 nm for (a), (b) the uniform SPAG and (c), (d) the rotated SPAG, respectively. The profiles (a), (c) and (b), (d) are obtained in $X-Z$ plane at projections and grooves of the SPAG, respectively. The white solid lines are the boundary line between different materials. The magnitudes of electric field intensity are indicated by the color scales.

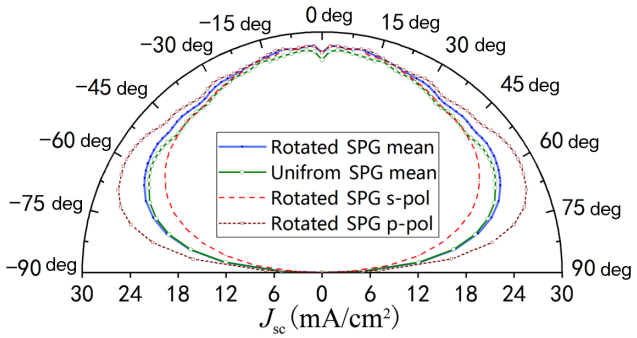

Fig. 8 The incident angle dependence of J_{sc} in both optimized rotated SPAG cell (for s, p, and average polarizations) and uniform SPAG cell (for average polarization).

more complex, indicating that multiple modes of light are excited. Moreover, in the Si layer of the rotated SPAG solar cell, large electric field intensities could be found. The phenomena are caused by the introduction of rotation disorders, which excite more quasiguided modes and leads to strong guided-mode resonances. Thus, it is consistent with the phenomena shown in Fig. 6. Furthermore, the electric field propagation direction of the rotated SPAG cell is inclined. Therefore, the optical path of the rotated SPAG should be longer than that of the uniform SPAG cell, which would also induce absorption enhancement. Therefore, from both diffraction and field analysis above, we can draw a conclusion that, with the introduction of rotation disorders, additional resonances would be excited, leading to both higher and additional absorption peaks.

3.5 *Angular Response and Structural Tolerance Analysis*

Given that the incident angle of sunlight to fixed solar cell constantly changes, understanding the absorption response at different incident angles is essential and important. Thus, the variation of J_{sc} of optimized rotated SPAG solar cell with different incident angles is investigated. For comparison, the characteristics of the incident angle of the reference uniform SPAG is also provided.

As shown in Fig. 8, for the averaged polarization, the incident angle characteristics of the two optimized SPAG solar cells are very similar overall. First, for each of the SPAG solar cells, J_{sc} of a small inclined incident angle range within ± 15 deg is higher than that at normal incidence (incident angle of 0 deg). Subsequently, with the continuous increase of the oblique angle, J_{sc} values of both SPAG cells are decreased with small fluctuation. Specifically, when the incident angle reaches the range from ± 46 deg to ± 55 deg, both J_{sc} values rise again slightly. Then, they will continue to decrease until the light is gone. As reported by previous investigations,[25,51] the increase of J_{sc} at small angles should be attributed to an increased possibility of coupling the incident light into resonances by breaking of the reflection symmetry at the oblique incidence. Next, the decreased J_{sc} is due to a decrease of the incidence power density at the cell surface with increased oblique angle. When the incident angle is about ± 55 deg, the J_{sc} values for both polarizations increase slightly, which can be explained by Fresnel formula, because the p-polarized light in that angle range has high absorptions. The phenomenon was also reported in the square nanowire array.[43] The above similar phenomena indicate that the basic characteristics of uniform SPAG cell are inherited by the rotated SPAG. Despite that, as shown in Fig. 8, there are also some differences between the incident angle characteristic curves of the two SPAG solar cells. Because of the rotation disorders, J_{sc} of the optimized rotated SPAG solar cell is always larger than that of the optimized uniform SPAG solar cell over the entire angle range. Moreover, within the incident angle range from 0 deg to 60 deg, a small decrease of 10.42% from the maximum J_{sc} could be observed for the uniform SPAG solar cell. An even smaller decrease from the maximum J_{sc} could be found for the rotated SPAG solar cell. Due to the broken symmetry by introducing rotation, the decrease rates in the rotated SPAG cells between from 0 deg to -60 deg and from 0 deg to 60 deg are different, which are 10.08% and 9.89%, respectively. Compared with the previously reported low-incidence sensitivity solar cell where the maximum

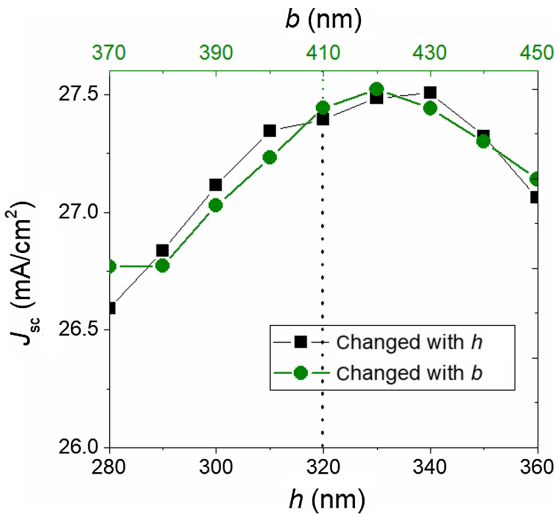

Fig. 9 J_{sc} of the rotated SPAG solar cell as functions of the h and b, respectively. The parameters h and b of optimized uniform SPAG are marked with dotted lines.

J_{sc} dropped by 11% in the same angle range,[51] our result shows that more stable angle absorption performance could be obtained in the proposed rotated SPAG solar cell.

In our previous investigation of finding the optimized rotation angle combination, the height h and width b of the square pillar in rotated SPAG cell are kept the same as the optimized h and b in the reference optimized uniform SPAG cell. However, they may not be optimal for the rotated SPAG cell. In fact, how h and b variations influence the absorption of the optimized rotated SPAG remains unknown. Thus, J_{sc} of the rotated SPAG cell as functions of h and b is investigated. As shown in Fig. 9, for the rotated SPAG cell when h deviates within ± 20 nm, the relative change rate of J_{sc} is from -1.02% to $+0.42\%$. Specially, when the h deviates within ± 10 nm, J_{sc} mildly changes by -0.048 to $+0.091$ mA/cm^2, which could be comparable to the previously reported high structural tolerance solar cell,[25] where the maximal J_{sc} decreases by 0.05 mA/cm^2. Therefore, efficient absorption in rotated SPAG cell could be mostly maintained in the case of small deviation of h, which can be controlled more accurately than b during the manufacturing. On the other hand, when b deviates within ± 20 nm, the relative change rate of J_{sc} is from -1.98% to $+0.37\%$. Compared with the previously reported solar cell where the maximum J_{sc} drops by 4.84% when projection width of grating is deviated by ± 11 nm,[15] the considerably smaller drop rate in the rotated SPAG cell shows that the absorption of rotated SPAG is well tolerant to the deviation of b. Therefore, the optimized rotated SPAG cell exhibits high tolerance with regard to both h and b deviations, manifesting that the absorption enhancement by the rotation disorders is robust. Moreover, it is noteworthy that when b increases by 10 nm or when h increases by 20 nm from their optimum, a slight larger J_{sc} could be observed. The phenomenon indicates that, after introducing the rotation disorder, the essential structural parameters (h and b) for the optimized uniform SPAG cell are not mostly appropriate for the rotated SPAG cell. Hence, by systematically considering the mutual influence of essential structural parameters and rotation angles (θ_i), the optical absorption of rotated SPAG would be further improved.

3.6 *Extension of Rotation in Spiral Grating*

The results above show that introducing rotation disorder is an effective method to improve absorption performance of the SPAG solar cells. In addition to the square pillars, could the rotation disorder also be effective to improve absorption in other existing common order grating solar cells? For example, rotation disorders are applied in this study to the previously reported spiral cell.[15] Except the rotation angles that are additionally introduced, all other structural parameters are taken from the literature,[15] in which the optimized spiral grating cell obtained

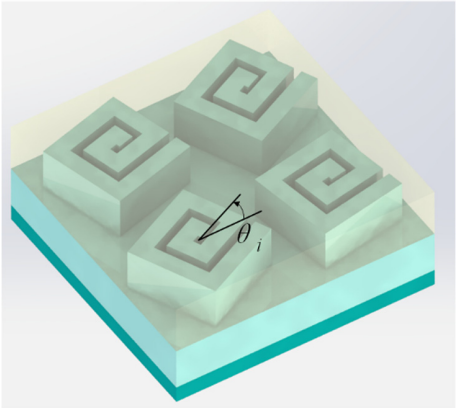

Fig. 10 Schematic view of rotated spiral grating.

an J_{sc} of 26.04 mA/cm^2. The same as what we did for the rotated SPAG cells above, rotation disorders are introduced in a 2×2 supercell spiral grating, as shown in Fig. 10.

As the spiral structure does not have the rotational symmetry, rotation of any angle would be a different case for solar cell. Therefore, finding various angles for each pillar possessing high absorption in such a wide rotation angle range is time-consuming. Thus, they are limited to a smaller range. Specifically, the rotation angle range considered is limited from 0 deg to 30 deg and with a step of 5 deg, within which the rotation angles for the spirals in the 2×2 supercell are generated. Only 60 sets of random rotation angle combinations are calculated. The maximum J_{sc} obtained is 26.50 mA/cm^2, which has the angle combination of 10 deg, 25 deg, 25 deg, and 10 deg. That means, compared with the original period spiral grating cell,[15] the rotated spiral grating cell obtains an absorption increase by 1.76%. If removing the angle rotation limitation, more probable disorder angle combinations from 0 deg to 360 deg would be introduced into the spiral texture. Thus, there may be additional opportunities to further increase absorption in rotated spiral grating solar. Moreover, since the absorption enhancement by introducing rotation in both SPAG and spiral grating cells is demonstrated, we could expect that the proposed method would be effective for any other single or composite structures, such as inverted pyramids[26] and asymmetric material pillar.[37]

4 Conclusions

Unlike adding local disorders by setting different shape parameters and/or changing the relative positions of the surface structures, the rotation is considered as a new degree of freedom in SPAG to obtain efficient and stable optical absorption solar cells. Compared with the unpatterned stack slab and the optimized uniform SPAG cells, enhanced absorptions of 78.54% and 3.21% are obtained in the optimized rotated SPAG, respectively. Moreover, at any oblique incidence angles, the absorption of the optimized rotated SPAG cell is always higher than that of the optimized uniform SPAG cell. These phenomena are mainly due to the introduction of rotation disorders, which not only diffract light into more orders, but also concentrate more diffraction energy onto those orders, exciting more quasiguided modes in the silicon absorption layer, and further resulting in an increase of absorption. Furthermore, both the low-incidence angular sensitivity and high structural tolerance indicate stable absorption performance for the proposed rotated SPAG cell. The maximum optical absorption only decreases by 10.08% within ± 60 deg oblique incidence range, and <2% absorption decrease is also found when the height or width of the subsquare pillar slightly deviates within ± 20 nm from the optimum. In addition, the result based on the spiral grating indicates that rotation disorders may also be beneficial to other single and composite structures. In sum, our study indicates that the proposed rotated SPAG would be promising to realize more efficient and stable light trapping. In addition, the way of introducing disorders through rotation, a new kind of disorder different from the conventional shape and relative position disorders would be promising for high absorption pseudounordered surface structures.

Acknowledgments

This work was supported by the National Natural Science Foundation of China (Grant No. 11504435); Natural Science Foundation of Hubei Province (Grant No. 2013CFA052); China Scholarship Council (Grant No. 201807780001); and the Fundamental Research Funds for the Central Universities, South-Central University for Nationalities, China.

References

1. X. Liu, Y. Da, and Y. Xuan, "Full-spectrum light management by pseudo-disordered moth-eye structures for thin film solar cells," *Opt. Express* **25**(16), A824–A839 (2017).
2. X. Meng et al., "Design, fabrication and optical characterization of photonic crystal assisted thin film monocrystalline-silicon solar cells," *Opt. Express* **20**(Suppl. 4), A465–A475 (2012).
3. F. Pratesi et al., "Disordered photonic structures for light harvesting in solar cells," *Opt. Express* **21**(Suppl. 3), A460–A468 (2013).
4. W. Zhang, L. Jiang, and X. Li, "Role of 2-D periodic symmetrical nanostructures in improving efficiency of thin film solar cells," *Opt. Commun.* **359**, 66–72 (2016).
5. W. I. Nam, Y. J. Yoo, and Y. M. Song, "Geometrical shape design of nanophotonic surfaces for thin film solar cells," *Opt. Express* **24**(14), A1033–A1044 (2016).
6. B. Bläsi et al., "3D optical simulation formalism OPTOS for textured silicon solar cells," *Opt. Express* **23**(24), A1720–A1734 (2015).
7. I. Kim et al., "Silicon nanodisk array design for effective light trapping in ultrathin c-Si," *Opt. Express* **22**(Suppl. 6), A1431–A1439 (2014).
8. Z. Jia et al., "Optical properties of a grating-nanorod assembly structure for solar cells," *Opt. Commun.* **376**, 14–20 (2016).
9. Y. Shi et al., "Nanopyramids and rear-located Ag nanoparticles for broad spectrum absorption enhancement in thin-film solar cells," *Opt. Express* **22**(17), 20473–20480 (2014).
10. J. Gjessing, A. S. Sudbø, and E. S. Marstein, "Comparison of periodic light-trapping structures in thin crystalline silicon solar cells," *J. Appl. Phys.* **110**(3), 033104 (2011).
11. C. Trompoukis et al., "Photonic assisted light trapping integrated in ultrathin crystalline silicon solar cells by nanoimprint lithography," *Appl. Phys. Lett.* **101**(10), 103901 (2012).
12. M. Chen et al., "Efficient light absorption in organic solar cells based on two-dimensional arrayed dielectric nanospheres," *IEEE Photonics J.* **8**(5), 1–9 (2016).
13. J. D. Winans et al., "Plasmonic effects in ultrathin amorphous silicon solar cells: performance improvements with Ag nanoparticles on the front, the back, and both," *Opt. Express* **23**(3), A92–A105 (2015).
14. F. Liu et al., "Plasmonic enhanced optical absorption in organic solar cells with metallic nanoparticles," *IEEE Photonics J.* **5**(4), 8400509 (2013).
15. J. Hou et al., "Biomimetic spiral grating for stable and highly efficient absorption in crystalline silicon thin-film solar cells," *Opt. Express* **25**(20), A922–A931 (2017).
16. Y. Zhang, B. Jia, and M. Gu, "Biomimetic and plasmonic hybrid light trapping for highly efficient ultrathin crystalline silicon solar cells," *Opt. Express* **24**(6), A506–A514 (2016).
17. D. Eisenhauer et al., "Honeycomb micro-textures for light trapping in multi-crystalline silicon thin-film solar cells," *Opt. Express* **26**(10), A498–A507 (2018).
18. A. Bozzola, M. Liscidini, and L. C. Andreani, "Broadband light trapping with disordered photonic structures in thin-film silicon solar cells," *Prog. Photovoltaics: Res. Appl.* **22**(12), 1237–1245 (2014).
19. M. S. Branham et al., "Empirical comparison of random and periodic surface light-trapping structures for ultrathin silicon photovoltaics," *Adv. Opt. Mater.* **4**(6), 858–863 (2016).
20. J. Li et al., "Spatial resolution effect of light coupling structures," *Sci. Rep.* **5**, 18500 (2015).
21. J. Xiao et al., "Paths to light trapping in thin film GaAs solar cells," *Opt. Express* **26**(6), A341–A351 (2018).
22. M. C. van Lare and A. Polman, "Optimized scattering power spectral density of photovoltaic light-trapping patterns," *ACS Photonics* **2**(7), 822–831 (2015).

23. E. R. Martins et al., "Deterministic quasi-random nanostructures for photon control," *Nat. Commun.* **4**, 2665 (2013).
24. S. Yu et al., "Design of non-deterministic quasi-random nanophotonic structures using Fourier space representations," *Sci. Rep.* **7**(1), 3752 (2017).
25. H. Ding et al., "Design rules for net absorption enhancement in pseudo-disordered photonic crystal for thin film solar cells," *Opt. Express* **24**(6), A650–A666 (2016).
26. J. Muller et al., "A fair comparison between ultrathin crystalline-silicon solar cells with either periodic or correlated disorder inverted pyramid textures," *Opt. Express* **23**(11), A657–A670 (2015).
27. L. Lalouat et al., "Pseudo-disordered structures for light trapping improvement in mono-crystalline Si thin-films," *Solar Energy Mater. Solar Cells* **159**, 649–656 (2017).
28. Y. Kawamoto et al., "Structural optimization of photonic crystals for enhancing optical absorption of thin film silicon solar cell structures," *IEEE Photonics J.* **6**(1), 1–10 (2014).
29. H. Ren et al., "Photonic quasicrystal nanopatterned silicon thin film for photovoltaic applications," *J. Opt.* **17**(3), 035901 (2015).
30. J. Xavier et al., "Quasicrystalline-structured light harvesting nanophotonic silicon films on nanoimprinted glass for ultra-thin photovoltaics," *Opt. Mater. Express* **4**(11), 2290–2299 (2014).
31. Y. Shi, X. Wang, and F. Yang, "Disorder improves light absorption in thin film silicon solar cells with hybrid light trapping structure," *Int. J. Opt.* **2016**, 1–8 (2016).
32. P. Li et al., "Analysis and optimisation of two-dimensional silicon complex grating with different ridge heights or groove depths for solar cells," in *ASME 2013 4th Int. Conf. Micro/Nanoscale Heat and Mass Transfer*, American Society of Mechanical Engineers (2013).
33. Y. Wu et al., "Broadband absorption enhancement in elliptical silicon nanowire arrays for photovoltaic applications," *Opt. Express* **22**(S5), A1292–A1302 (2014).
34. X. Qin et al., "Enhanced light absorption in perpendicular elliptical silicon nanocone array for solar cells," *Appl. Opt.* **56**(8), 2307–2313 (2017).
35. S. J. Han et al., "Symmetry-breaking nanostructures on crystalline silicon for enhanced light trapping in thin film solar cells," *Opt. Express* **24**(26), A1586–A1596 (2016).
36. A. Ghobadi et al., "Visible light nearly perfect absorber: an optimum unit cell arrangement for near absolute polarization insensitivity," *Opt. Express* **25**(22), 27624–27634 (2017).
37. R. Lin and X. Li, "Multifocal metalens based on multilayer Pancharatnam–Berry phase elements architecture," *Opt. Lett.* **44**, 2819 (2019).
38. I. Kim et al., "Asymmetric back contact nanograting design for thin c-Si solar cells," *Curr. Appl. Phys.* **16**(5), 568–573 (2016).
39. N. A. Yahaya et al., "Characterization of light absorption in thin-film silicon with periodic nanohole arrays," *Opt. Express* **21**(5), 5924–5930 (2013).
40. T. A. König et al., "Electrically tunable plasmonic behavior of nanocube-polymer nanomaterials induced by a redox-active electrochromic polymer," *ACS Nano* **8**(6), 6182–6192 (2014).
41. K. M. McPeak et al., "Plasmonic films can easily be better: rules and recipes," *ACS Photonics* **2**(3), 326–333 (2015).
42. M. A. Green, "Self-consistent optical parameters of intrinsic silicon at 300 K including temperature coefficients," *Solar Energy Mater. Solar Cells* **92**(11), 1305–1310 (2008).
43. X. Fang, C. Y. Zhao, and H. Bao, "Radiative behaviors of crystalline silicon nanowire and nanohole arrays for photovoltaic applications," *J. Quant. Spectrosc. Radiat. Transfer* **133**, 579–588 (2014).
44. T. K. Chong et al., "Optimal wavelength scale diffraction gratings for light trapping in solar cells," *J. Opt.* **14**(2), 024012 (2012).
45. V. Liu and S. Fan, "S4: a free electromagnetic solver for layered periodic structures," *Comput. Phys. Commun.* **183**(10), 2233–2244 (2012).
46. T.-G. Chen et al., "Characteristics of large-scale nanohole arrays for thin-silicon photovoltaics," *Prog. Photovoltaics: Res. Appl.* **22**(4), 452–461 (2014).
47. American Society for Testing Materials (ASTM), "Source of data ASTM/NREL," https://www.nrel.gov/grid/solar-resource/spectra-am1.5.html (2012).

48. K. R. Catchpole and M. A. Green, "A conceptual model of light coupling by pillar diffraction gratings," *J. Appl. Phys.* **101**(6), 063105 (2007).
49. E. Yablonovitch and G. D. Cody, "Intensity enhancement in textured optical sheets for solar cells," *IEEE Trans. Electron Devices* **29**(2), 300–305 (1982).
50. Q. G. Du et al., "Broadband absorption enhancement in randomly positioned silicon nanowire arrays for solar cell applications," *Opt. Lett.* **36**(10), 1884–1886 (2011).
51. J. Gjessing, E. S. Marstein, and A. Sudbø, "2D back-side diffraction grating for improved light trapping in thin silicon solar cells," *Opt. Express* **18**(6), 5481–5495 (2010).

Biographies of the authors are not available.